Predictions for neutron stars from holographic nuclear matter

Nicolas Kovensky[1], Aaron Poole[2] and Andreas Schmitt[2⋆]

1 Institut de Physique Théorique, Université Paris Saclay, CEA, CNRS, Orme des Merisiers, 91191 Gif-sur-Yvette CEDEX, France.
2 Mathematical Sciences and STAG Research Centre, University of Southampton, Southampton SO17 1BJ, United Kingdom

⋆ a.schmitt@soton.ac.uk

Proceedings for the XXXIII International Workshop on High Energy Physics, Hard Problems of Hadron Physics: Non-Perturbative QCD & Related Quests ONLINE, 8-12 November 2021
doi:10.21468/SciPostPhysProc.6

Abstract

We discuss masses, radii, and tidal deformabilities of neutron stars constructed from the holographic Witten-Sakai-Sugimoto model. Using the same model for crust and core of the star, we combine our theoretical results with the latest astrophysical data, thus deriving more stringent constraints than given by the data alone. For instance, our calculation predicts – independent of the model parameters – an upper limit for the maximal mass of the star of about 2.46 solar masses and a lower limit of the (dimensionless) tidal deformability of a 1.4-solar-mass star of about 277.

Received 31-01-2022
Accepted 06-05-2022
Published 31-05-2022
doi:10.21468/SciPostPhysProc.6.019

1 Introduction

The gauge-gravity duality [1,2] is a powerful non-perturbative tool to understand strongly coupled gauge theories. Based on the holographic principle, it is employed to obtain otherwise inaccessible strong-coupling results from classical gravity calculations in higher dimensions. Here we use a certain realization of the gauge-gravity duality, the Witten-Sakai-Sugimoto model [2–4], to describe cold and dense matter at baryon and isospin densities relevant for neutron stars.

Neutron stars present a unique laboratory for matter at large, but not asymptotically large, densities, where first-principle calculations within Quantum Chromodynamics (QCD) are too difficult within currently available techniques (for recent progress on the lattice see for instance Refs. [5–7]). The interior of neutron stars is therefore often studied with the help of phenomenological models, effective field theories, or extrapolations of perturbative results, and the resulting thermodynamic and transport properties can be linked to astrophysical observables [8,9]. In recent years, an increasing amount of astrophysical data has become available,

for instance through the detection of gravitational waves from neutron star mergers [10, 11] and through the NICER mission [12–15]. We shall combine the inferred estimates for mass, radius, and tidal deformability of neutron stars with our holographic calculation.

The Witten-Sakai-Sugimoto model is the holographic top-down approach – based on type-IIA string theory – that is closest to real-world QCD. It accounts for chiral and deconfinement phase transitions, and several candidate phases at high densities can be realized, including a holographic version of quarkyonic matter [16], which, however, tends to appear at densities larger than expected in the cores of neutron stars. Here we restrict ourselves to nuclear matter with two flavors, $N_f = 2$, i.e., hybrid stars with a quark matter core or a quarkyonic core will not be discussed. We employ the holographic results for the core of the star and, within a simple approximation, for the crust as well, such that the crust-core transition is determined dynamically. In this regard, our study goes beyond previous holographic approaches to neutron stars [17–20] and beyond many field-theoretical studies, where the crust is often obtained from a separate approach and assumptions about the crust-core transition have to be added by hand. Different holographic approaches have recently been reviewed and compared in Ref. [21].

Secs. 2 and 3.1 of these proceedings provide a review of the results of Ref. [22]. However, we significantly enhance these results by combining them more systematically with the astrophysical data, thus extracting novel predictions for mass, radius, and tidal deformability of the star in Sec. 3.2.

2 Holographic approach

2.1 Model and approximations

We work within the background geometry of the Witten-Sakai-Sugimoto model that corresponds to the confined phase. The background is given by N_c D4-branes, where N_c corresponds to the number of colors in the dual gauge theory. The N_f D8- and $\overline{\text{D8}}$-branes, added to describe left- and right-handed fermions [3, 4], are assumed to be maximally separated asymptotically in a compact extra dimension with radius M_{KK}^{-1}, such that their embedding in the bulk follows geodesics. In this version of the model, there are only two parameters: the 't Hooft coupling λ and the Kaluza-Klein mass M_{KK}, and we shall discuss our results in this parameter space systematically (setting $N_c = 3$, $N_f = 2$). We approximate the Dirac-Born-Infeld part of the gauge field action on the flavor branes by the Yang-Mills action. The Chern-Simons part of the action is crucial to implement nonzero baryon number, and we shall introduce baryonic matter within the "homogeneous ansatz" [23,24]. In this ansatz, the spatial components of the non-abelian part of the gauge field are assumed to depend only on the holographic (radial) coordinate, not on the spatial ones. In contrast to an instantonic approach [25, 26], this approximation is expected to be justified at sufficiently large baryon densities. All our results are valid at zero temperature. For the details of the theoretical setup see Ref. [27], where it was shown how to include an isospin chemical potential in the presence of baryonic matter. This is crucial for the description of realistic neutron star matter. In Ref. [27], pion condensation was also included and its competition and coexistence with nuclear matter in the phase diagram was investigated. Here we ignore pion condensation for simplicity. We also neglect the current quark masses (since we only discuss non-strange matter, this is a very good approximation in our context), whose effect on the phase structure in the present model was studied in Refs. [16, 28]. The holographic nuclear matter thus constructed shares several properties with real-world nuclear matter, such as a first-order baryon onset of isospin-symmetric nuclear matter. A caveat of the approximation arises due to the semi-classical large-N_c treatment of the baryons. In this treatment, the isospin spectrum is continuous, and neutron and proton

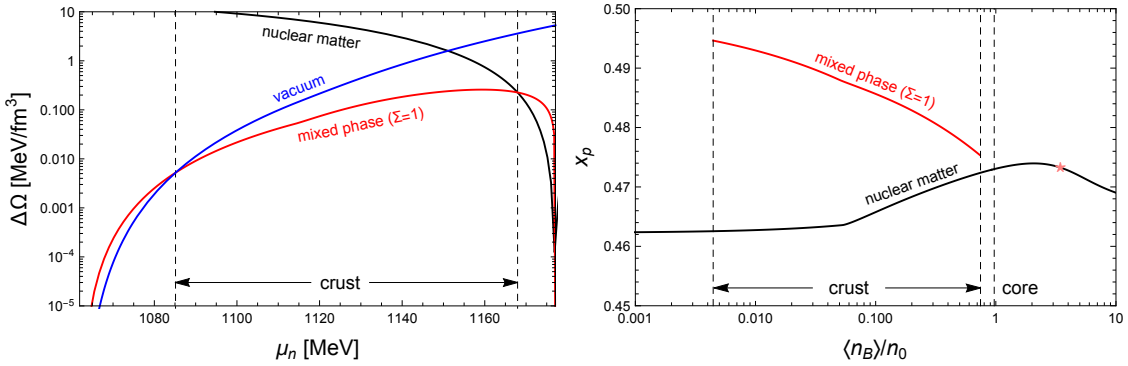

Figure 1: *Left panel:* Free energy densities relative to the mixed phase without Coulomb and surface effects as a function of the neutron chemical potential. The surface tension is set to $\Sigma = 1\,\mathrm{MeV/fm^2}$. *Right panel:* Corresponding proton fraction as a function of the spatially averaged baryon density, normalized by the saturation density of nuclear matter. The star indicates the density and proton fraction in the center of the most massive star. For both panels, $\lambda = 10$, $M_{\mathrm{KK}} = 949\,\mathrm{MeV}$, resulting in a saturation density $n_0 \simeq 0.21\,\mathrm{fm}^{-3}$, somewhat larger than in QCD.

states are not explicitly present. While we can still identify the two isospin components with the neutron and the proton, the continuous spectrum is responsible for a symmetry energy at saturation density that is an order of magnitude larger than in the real world. We shall see momentarily that this results in a very large proton fraction of our neutron star matter.

2.2 Holographic crust

We combine our holographic nuclear matter with a lepton gas made of electrons and muons. Requiring equilibrium with respect to the electroweak interaction and local charge neutrality defines the spatially homogeneous matter in the neutron star core. We also allow for a mixed phase of nuclear matter (plus leptons) and a lepton gas. For the construction of this mixed phase – which forms the crust of the neutron star – we require global charge neutrality and assume the interfaces between the two phases to be sharp surfaces. This assumption requires us to introduce the surface tension of nuclear matter Σ as an additional external parameter. We assume Σ to be constant throughout the crust and will mostly use $\Sigma = 1\,\mathrm{MeV/fm^2}$, which is a realistic value for symmetric nuclear matter at saturation density (roughly the density of our nuclear matter clusters in the crust, up to the crust-core transition). Moreover, we employ the Wigner-Seitz approximation and restrict ourselves to the spherical geometry, i.e., we only consider spherical bubbles of nuclear matter (with dynamically determined size and composition) immersed in a lepton gas, as expected for the outer crust of the star. We do not construct a mixed phase of nuclear matter with pure neutron matter, as expected for the inner crust. After these simplifications, the holographic equations of motion together with the neutrality and beta-equilibrium conditions yield the preferred phase for any neutron chemical potential μ_n fully dynamically.

We show the results for a certain parameter set in Fig. 1. The left panel compares the free energy densities of the vacuum, homogeneous nuclear matter, and the mixed phase including Coulomb and surface effects to the free energy density of the mixed phase without Coulomb and surface effects. We read off the transitions between the vacuum and the mixed phase (this will correspond to the surface of the star) and the transition from the mixed phase to homogeneous nuclear matter (crust-core transition). The right panel shows the corresponding proton fraction $x_p = n_p/n_B$, where n_p and n_B are proton and baryon number densities,

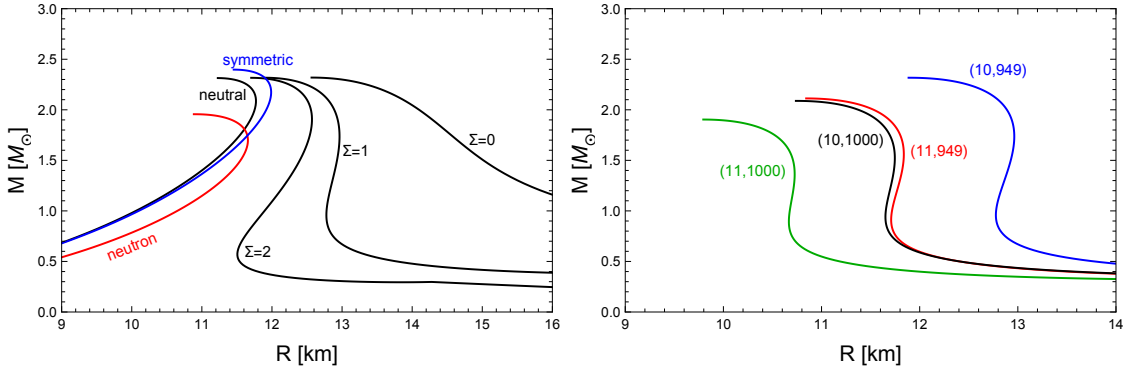

Figure 2: *Left panel:* Black curves show the effect of the crust, from no crust at all (left) through crust with Coulomb and surface effects (middle, surface tension as labeled, in units of MeV/fm^2) to crust without energy cost (right). For comparison, also the curves for symmetric nuclear matter and pure neutron matter are shown (blue and red, both without crust). In this panel, $\lambda = 10$, $M_{\rm KK} = 949$. *Right panel:* Mass-radius curves including the crust with $\Sigma = 1\,\text{MeV/fm}^2$ for different model parameters λ and $M_{\rm KK}$ (in MeV), as labeled. All curves end at the maximal mass, beyond which the stars are unstable with respect to radial oscillations.

respectively. We see that our nuclear matter evolves from almost symmetric nuclear matter to more asymmetric matter as we approach the crust-core transition. Then, in the core of the star, the proton fraction rises until at ultra-high densities it decreases again. We also see that the values for x_p are close to 0.5 throughout. This indicates that there is a large energy cost associated with creating isospin-asymmetric matter, which can be attributed to the large-N_c approximation of our approach. Improving the approach to overcome this unrealistic feature is an important step for future work.

3 Holographic neutron stars

3.1 Mass-radius curves

The holographic calculation laid out in the previous section provides us with all thermodynamic quantities. We can thus straightforwardly compute the equation of state, i.e., the pressure as a function of energy density, including the first-order phase transition at the crust-core boundary, and the corresponding speed of sound. Equation of state and speed of sound are then used as input for the Tolman-Oppenheimer-Volkoff equations (supplemented by an equation for the perturbation of the metric due to tidal deformations), which are solved numerically to extract gravitational mass M, radius R, and tidal deformability Λ for a given central pressure of the star. Varying the central pressure yields mass-radius relations as presented in Fig. 2. The left panel of this figure shows the effect of the crust and different surface tensions: ignoring the crust leads to very small radii, a crust without Coulomb and surface effects yields very large radii (then the crust is unrealistically large), while Coulomb and surface effects render the effect of the crust more moderate, resulting in radii between the two extremes. The maximal mass is almost unaffected by these changes. The left panel also shows the comparison with pure neutron matter and isospin-symmetric nuclear matter. For the right panel, we have fixed the surface tension and have varied the model parameters λ and $M_{\rm KK}$. This panel suggests that realistic "holographic stars" can be obtained. In particular, masses above $2.1\,M_\odot$, where $M_\odot$ is the solar mass, are reached, which is a necessary requirement on account of the observation

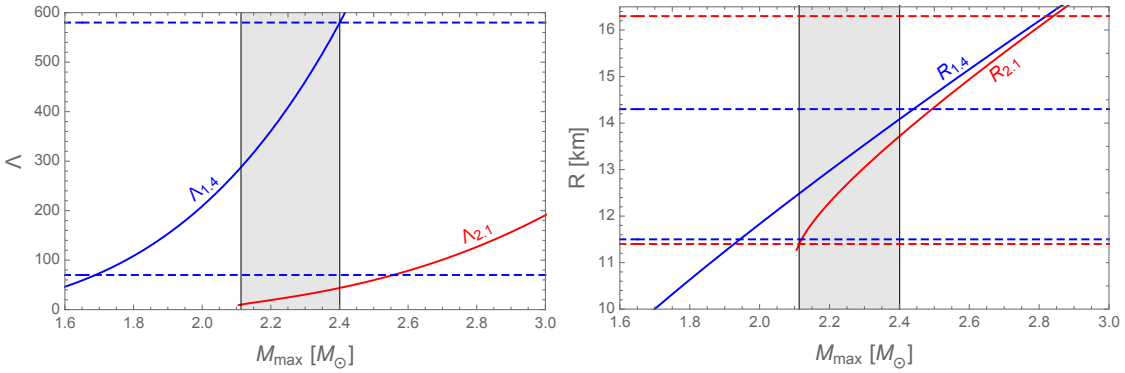

Figure 3: Tidal deformability Λ and radius R for a 1.4-solar-mass star (blue solid) and a 2.1-solar-mass star (red solid) as a function of the maximal mass $M_{\max}$. Here we have fixed the 't Hooft coupling $\lambda = 10$ and the surface tension $\Sigma = 1\,\mathrm{MeV/fm}^2$, and different values of $M_{\max}$ are obtained by varying the second model parameter M_{KK}. The horizontal dashed lines indicate the astrophysical constraints for $\Lambda_{1.4}$, $R_{1.4}$, and $R_{2.1}$. Beyond the shaded region at least one of the constraints is violated. As a consequence, for this particular value of the 't Hooft coupling, we obtain $2.11\,M_\odot \lesssim M_{\max} \lesssim 2.40\,M_\odot$ and new bounds for $\Lambda_{1.4}$, $R_{1.4}$, $\Lambda_{2.1}$, $R_{2.1}$, for instance $288 \lesssim \Lambda_{1.4} \lesssim 580$.

of the heaviest known neutron star [29]. We shall confront our results with the other known constraints in the next subsection and see that indeed all known astrophysical constraints can be satisfied (in contrast to the simple pointlike approximation of baryons within the same holographic model [22, 30]).

3.2 Combining holographic results with astrophysical constraints

Besides the existence of a 2.1-solar-mass star, we also consider the constraints for the tidal deformability, $70 < \Lambda_{1.4} < 580$ [10], and radius, $11.5\,\mathrm{km} < R_{1.4} < 14.3\,\mathrm{km}$ (putting together Refs. [12,13]), of a (roughly) 1.4-solar-mass star as well as the radius, $11.4\,\mathrm{km} < R_{2.1} < 16.3\,\mathrm{km}$ (putting together Refs. [14, 15]), of a (roughly) 2.1-solar-mass star. We demonstrate in Fig. 3 how these constraints can be combined with our holographic results to derive more stringent conditions for mass, radius, and tidal deformability. To obtain this figure, we have fixed the 't Hooft coupling λ and calculated the properties of 1.4-solar-mass and 2.1-solar-mass stars and the maximal mass $M_{\max}$ for different values of M_{KK}. This results in the red and blue solid curves (the curves for the $2.1\,M_\odot$ star obviously end where the maximal mass drops below that value). Since the microscopic calculation of homogeneous nuclear matter becomes independent of M_{KK} in the absence of any additional energy scale, we have ignored the muon contribution and set the electron mass to zero here and for the following results. (The surface tension does introduce another energy scale and thus a dependence on M_{KK}, but its effect is computed without much numerical effort once the main holographic calculation for a given λ is done.) We now compare the solid curves with the astrophysical constraints, indicated by the horizontal dashed lines. It turns out that the strongest constraint for the upper limit of $M_{\max}$ is the upper limit of $\Lambda_{1.4}$ while the strongest constraint for the lower limit of $M_{\max}$ is the lower limit of $R_{2.1}$. This gives the two vertical lines, which define the shaded region. This region, in turn, gives new upper limits for $R_{1.4}$, $R_{2.1}$, and new lower limits for $R_{1.4}$, $\Lambda_{1.4}$ (as well as upper and lower limits for $\Lambda_{2.1}$, for which no constraints are known).

The shaded region also yields an "astrophysically allowed" range for the second model parameter M_{KK} because each $M_{\max}$ in Fig. 3 is generated by choosing a value for M_{KK}. Repeating

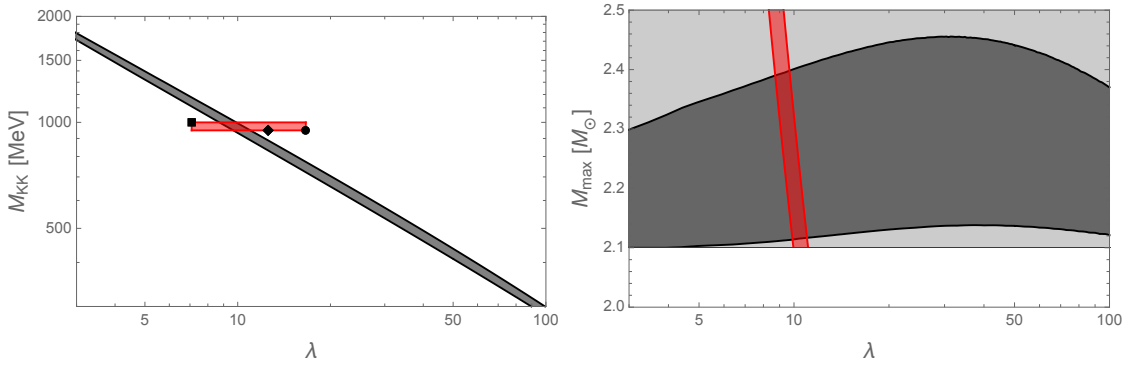

Figure 4: *Left panel:* Allowed range according to the astrophysical constraints in the λ-M_{KK} plane (doubly logarithmic), obtained by applying the construction of Fig. 3 for each λ. The three symbols mark the parameter pairs from the QCD fits of table 1, and we use them to define a "QCD window" (red). *Right panel:* Constraints for the maximal mass of the neutron star as a function of the 't Hooft coupling λ. The light gray band gives the constraint from astrophysical data. The dark gray band and the red band arise from applying the constraints of the left panel.

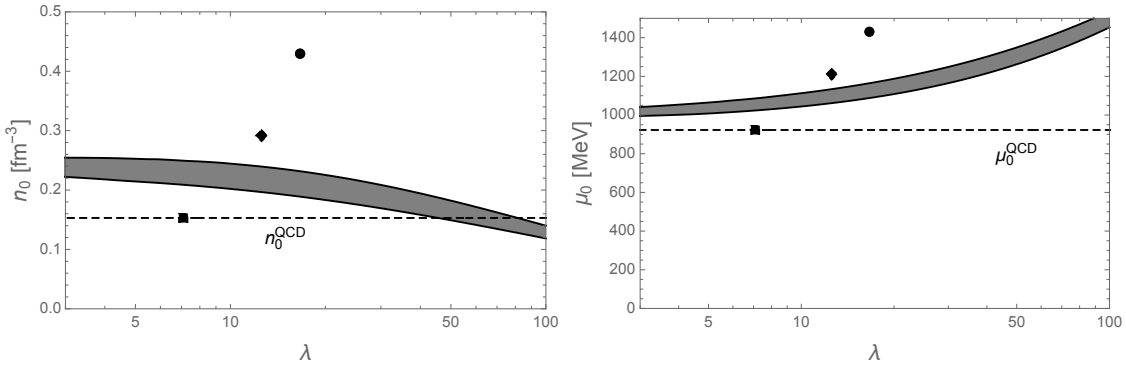

Figure 5: Saturation density of symmetric nuclear matter (left) and corresponding onset chemical potential (right) as functions of λ for the astrophysically allowed parameter band, see left panel of Fig. 4, and for the three fits of table 1. The dashed horizontal lines indicate the real-world values.

this calculation for many values of λ we can thus determine a window in the M_{KK}-λ plane that satisfies all astrophysical constraints. For most of the λ range we consider, the situation is qualitatively the same as in Fig. 3. For very small λ, however, the scenario slightly differs: Instead of the lower bound for $R_{2.1}$, the existence of the 2.1-solar-mass star becomes the strongest constraint for the lower bound of M_{max}; and instead of the upper bound for $\Lambda_{1.4}$, the upper bound for $R_{1.4}$ becomes the strongest constraint for the upper bound of M_{max}. The resulting window is the gray shaded area in the left panel of Fig. 4. For comparison, we have indicated three particular parameter choices obtained from fits to QCD vacuum properties (circle and diamond) and to saturation properties of symmetric nuclear matter (square), as explained in table 1. We see that these three points do not coincide and none of them lies in the astrophysically allowed band. Having in mind that the points and the band are constructed to fit properties of vastly different systems, it is perhaps not surprising that the Witten-Sakai-Sugimoto model, at least in the simple version employed here, cannot account for all of them simultaneously. To get some further idea of the extent by which the properties of nuclear matter are violated, we have plotted the saturation density n_0 and the onset chemical potential μ_0 for the astro-

Table 1: Fits of the model parameters to vacuum properties (pion decay constant and rho meson mass [3,4], first row, QCD string tension and rho meson mass [31], second row), and to nuclear saturation properties (saturation density $n_0 = 0.153\,\mathrm{fm}^{-3}$ and onset chemical potential $\mu_0 = 922.7\,\mathrm{MeV}$ of symmetric nuclear matter, third row, this work).

fit to	λ	M_{KK}	Figs. 4, 5
f_π, m_ρ	16.63	949 MeV	●
σ, m_ρ	12.55	949 MeV	♦
n_0, μ_0	7.09	1000 MeV	■

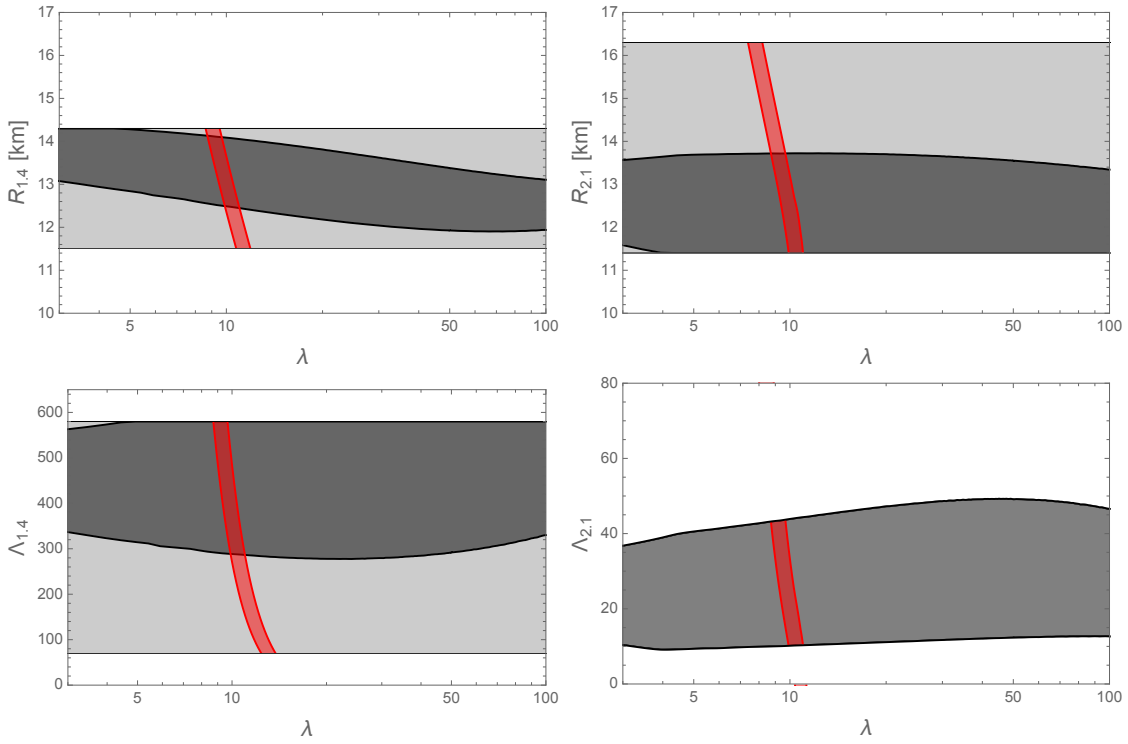

Figure 6: Same as right panel of Fig. 4, but for radius and deformability of 1.4-solar-mass and 2.1-solar-mass stars.

physically allowed band and the three separate fits in Fig. 5. If we are more modest and do not require to fit "everything" with a single parameter set but at least keep the QCD properties approximately correct, it is useful to define a "QCD window", given by the fits to the vacuum and nuclear matter: $M_{\mathrm{KK}} \simeq (949-1000)\,\mathrm{MeV}$ and $\lambda \simeq 7-17$. We have indicated this window as a red rectangle in the left panel of Fig. 4.

In the right panel of this figure and in Fig. 6 we collect the constraints for all λ obtained from the construction of Fig. 3. Constraints from astrophysical data alone are shown by a light gray band (obviously independent of the microscopic model parameter λ). The panel for the deformability $\Lambda_{2.1}$ does not have such a band because there is no data available from a neutron star merger with a star of that mass. The dark gray bands are the more stringent constraints obtained by combining the data with the results of the model. They allow us to read off predictions of the model that are completely general, i.e., with no assumptions about the model parameters λ and M_{KK} (for a fixed value of the surface tension in the crust). We have collected these predictions in table 2. For the "parameter-independent" bounds we have used the upper or lower limits of the bands visible in the plots. In all cases, perhaps with

Table 2: Constraints obtained by combining the holographic results with astrophysical data for maximal mass as well as radius and tidal deformability for 1.4-solar-mass and 2.1-solar-mass stars. Parameter-independent bounds are valid for any model parameters λ, M_{KK}, while the QCD window defined by table 1 and Fig. 4 gives tighter bounds. Parentheses indicate that our model does not further restrict the astrophysical data used here.

	parameter independent		QCD window	
	lower bound	upper bound	lower bound	upper bound
$M_{\mathrm{max}}\,[M_\odot]$	(2.1)	2.46	2.11	2.40
$R_{1.4}\,[\mathrm{km}]$	11.9	(14.3)	12.4	14.1
$R_{2.1}\,[\mathrm{km}]$	(11.4)	13.7	(11.4)	13.7
$\Lambda_{1.4}$	277	(580)	286	(580)
$\Lambda_{2.1}$	9.13	49.3	10.1	43.7

the exception of $\Lambda_{2.1}$, the shapes of the bands suggest that these are the general bounds even beyond the shown λ regime. Our predictions can further be refined by focusing on the QCD window, which is shown in each panel as a red band (cut off at the boundaries of the light gray band). The steepness of the red bands indicate that the observables are very sensitive to variations in λ. The refined constraints are then obtained from the intersections of the red bands with the dark gray bands (more precisely the upper or lower corner of the intersection, depending on whether we obtain an upper or lower limit). These values are also collected in table 2. For instance, we find as a general prediction of the model that neutron stars cannot be heavier than 2.46 solar masses, while if we are interested to approximately reproduce vacuum and nuclear matter properties at the same time, this upper limit can be lowered to 2.40 solar masses. Similarly, for any parameter values the tidal deformability of a 1.4-solar-mass star cannot be lower than 277, the QCD window further narrows this down to a lower limit of about 286.

4 Conclusion

We have employed a holographic description of zero-temperature, high-density nuclear matter and used this single, top-down formalism to construct neutron stars. In particular, since our holographic nuclear matter is allowed to become isospin asymmetric, we were able to account for electroweak equilibrium and electric charge neutrality, and we have constructed a mixed phase of nuclear matter and a lepton gas to include the crust of the star fully dynamically. We have demonstrated that the model can reproduce realistic neutron stars, and we have combined our microscopic results with the latest astrophysical data to derive constraints for mass, radius, and tidal deformability of the star.

Improvements of the holographic model are necessary for more reliable predictions, most notably a refined approximation regarding the isospin spectrum is highly desired. More straightforward improvements of the present calculation would be the construction of an inner crust as a mixed phase of pure neutron matter and nearly symmetric nuclear matter, taking into account different geometrical structures in the crust and the crust-core transition region, and computing the surface tension dynamically within the model. Other extensions are the inclusion of strangeness (and a nonzero strange quark mass), pion condensation, nonzero temperature effects, a magnetic field, and the phase transition to a chirally restored phase. Most of these ingredients have been developed already within the given model and have to be com-

bined and possibly improved for neutron star applications. It would also be interesting to use the model to compute transport properties, as recently done in the context of dense matter within different holographic setups [32, 33].

Acknowledgements

We thank N. Jokela and A. Rebhan for valuable comments. A.P. is supported by an Engineering and Physical Sciences Research Council (EPSRC) Mathematical Sciences Fellowship at the University of Southampton. N.K. is supported by the ERC Consolidator Grant 772408-Stringlandscape.

References

[1] J. M. Maldacena, *The Large N limit of superconformal field theories and supergravity*, Adv. Theor. Math. Phys. **2**, 231 (1998), doi:10.1023/A:1026654312961.

[2] E. Witten, *Anti-de Sitter Space, Thermal Phase Transition, And Confinement In Gauge Theories*, arXiv:hep-th/9803131.

[3] T. Sakai and S. Sugimoto, *Low Energy Hadron Physics in Holographic QCD*, Prog. Theor. Phys.**113**, 843 (2005), doi:10.1143/PTP.113.843.

[4] T. Sakai and S. Sugimoto, *More on a Holographic Dual of QCD*, Prog. Theor. Phys. **114**, 1083 (2005), doi:10.1143/PTP.114.1083.

[5] O. Philipsen and J. Scheunert, *QCD in the heavy dense regime for general Nc: on the existence of quarkyonic matter*, J. High Energy Phys. **11**, 022 (2019), doi:10.1007/JHEP11(2019)022.

[6] Y. Ito, H. Matsufuru, Y. Namekawa, J. Nishimura, S. Shimasaki, A. Tsuchiya and S. Tsutsui, *Complex Langevin calculations in QCD at finite density*, J. High Energy Phys. **10**, 144 (2020), doi:10.1007/JHEP10(2020)144.

[7] S. Borsányi, Z. Fodor, J. N. Guenther, R. Kara, S. D. Katz, P. Parotto, A. Pásztor, C. Ratti and K. K. Szabó, *Lattice QCD Equation of State at Finite Chemical Potential from an Alternative Expansion Scheme*, Phys. Rev. Lett. **126**, 232001 (2021), doi:10.1103/PhysRevLett.126.232001.

[8] A. Schmitt, *Dense Matter in Compact Stars*, Springer Berlin Heidelberg, ISBN 9783642128653 (2010), doi:10.1007/978-3-642-12866-0.

[9] A. Schmitt and P. Shternin, *Reaction Rates and Transport in Neutron Stars*, in The Physics and Astrophysics of Neutron Stars, Springer International Publishing, Cham, ISBN 9783319976150 (2018), doi:10.1007/978-3-319-97616-7_9.

[10] B. P. Abbott et al., *Properties of the Binary Neutron Star Merger GW170817*, Phys. Rev. X **9**, 011001 (2019), doi:10.1103/PhysRevX.9.011001.

[11] R. Abbott et al., *GW190814: Gravitational Waves from the Coalescence of a 23 Solar Mass Black Hole with a 2.6 Solar Mass Compact Object*, Astrophys. J. Lett. **896**, L44 (2020), doi:10.3847/2041-8213/ab960f.

[12] T. E. Riley et al., *A NICER View of PSR J0030+0451: Millisecond Pulsar Parameter Estimation*, Astrophys. J. Lett. **887**, L21 (2019), doi:10.3847/2041-8213/ab481c.

[13] M. C. Miller et al., *PSR J0030+0451 Mass and Radius from NICER Data and Implications for the Properties of Neutron Star Matter*, Astrophys. J. Lett. **887**, L24 (2019), doi:10.3847/2041-8213/ab50c5.

[14] T. E. Riley et al., *A NICER View of the Massive Pulsar PSR J0740+6620 Informed by Radio Timing and XMM-Newton Spectroscopy*, Astrophys. J. Lett. **918**, L27 (2021), doi:10.3847/2041-8213/ac0a81.

[15] M. C. Miller et al., *The Radius of PSR J0740+6620 from NICER and XMM-Newton Data*, Astrophys. J. Lett. **918**, L28 (2021), doi:10.3847/2041-8213/ac089b.

[16] N. Kovensky and A. Schmitt, *Holographic quarkyonic matter*, J. High Energy Phys. **09**, 112 (2020), doi:10.1007/JHEP09(2020)112.

[17] C. Hoyos, N. Jokela, D. Rodríguez Fernández and A. Vuorinen, *Holographic Quark Matter and Neutron Stars*, Phys. Rev. Lett. **117**, 032501 (2016), doi:10.1103/PhysRevLett.117.032501.

[18] N. Jokela, M. Järvinen and J. Remes, *Holographic QCD in the Veneziano limit and neutron stars*, J. High Energy Phys. **03**, 041 (2019), doi:10.1007/JHEP03(2019)041.

[19] K. Bitaghsir Fadafan, J. Cruz Rojas and N. Evans, *Holographic quark matter with color superconductivity and a stiff equation of state for compact stars*, Phys. Rev. D **103**, 026012 (2021), doi:10.1103/PhysRevD.103.026012.

[20] N. Jokela, M. Järvinen, G. Nijs and J. Remes, *Unified weak and strong coupling framework for nuclear matter and neutron stars*, Phys. Rev. D **103**, 086004 (2021), doi:10.1103/PhysRevD.103.086004.

[21] C. Hoyos, N. Jokela and A. Vuorinen, *Holographic approach to compact stars and their binary mergers*, arXiv:2112.08422.

[22] N. Kovensky, A. Poole and A. Schmitt, *Building a realistic neutron star from holography*, Phys. Rev. D **105**, 034022 (2022), doi:10.1103/PhysRevD.105.034022.

[23] M. Rozali, H.-H. Shieh, M. Van Raamsdonk and J. Wu, *Cold nuclear matter in holographic QCD*, J. High Energy Phys. **01**, 053 (2008), doi:10.1088/1126-6708/2008/01/053.

[24] S.-w. Li, A. Schmitt and Q. Wang, *From holography towards real-world nuclear matter*, Phys. Rev. D **92**, 026006 (2015), doi:10.1103/PhysRevD.92.026006.

[25] F. Preis, A. Rebhan and A. Schmitt, *Holographic baryonic matter in a background magnetic field*, J. Phys. G: Nucl. Part. Phys. **39**, 054006 (2012), doi:10.1088/0954-3899/39/5/054006.

[26] K. Bitaghsir Fadafan, F. Kazemian and A. Schmitt, *Towards a holographic quark-hadron continuity*, J. High Energy Phys. **03**, 183 (2019), doi:10.1007/JHEP03(2019)183.

[27] N. Kovensky and A. Schmitt, *Isospin asymmetry in holographic baryonic matter*, SciPost Phys. **11**, 029 (2021), doi:10.21468/SciPostPhys.11.2.029.

[28] N. Kovensky and A. Schmitt, *Heavy holographic QCD*, J. High Energy Phys. **02**, 096 (2020), doi:10.1007/JHEP02(2020)096.

[29] H. T. Cromartie et al., *Relativistic Shapiro delay measurements of an extremely massive millisecond pulsar*, Nat. Astron. **4**, 72 (2019), doi:10.1038/s41550-019-0880-2.

[30] K. Zhang, T. Hirayama, L.-W. Luo and F.-L. Lin, *Compact star of holographic nuclear matter and GW170817*, Phys. Lett. B **801**, 135176 (2020), doi:10.1016/j.physletb.2019.135176.

[31] F. Brünner, D. Parganlija and A. Rebhan, *Glueball decay rates in the Witten-Sakai-Sugimoto model*, Phys. Rev. D **91**, 106002 (2015), doi:10.1103/PhysRevD.91.106002.

[32] C. Hoyos, M. Järvinen, N. Jokela, J. G. Subils, J. Tarrío and A. Vuorinen, *Transport in Strongly Coupled Quark Matter*, Phys. Rev. Lett. **125**, 241601 (2020), doi:10.1103/PhysRevLett.125.241601.

[33] C. Hoyos, N. Jokela, M. Järvinen, J. G. Subils, J. Tarrío and A. Vuorinen, *Holographic approach to transport in dense QCD matter*, Phys. Rev. D **105**, 066014 (2022), doi:10.1103/PhysRevD.105.066014.